Acquisition of photoelectron diffraction patterns with a two-dimensional wide-angle electron analyzer

Greif, Michael ; Castiglioni, Luca ; Becker-Koch, David ; Osterwalder, Jürg ; Hengsberger, Matthias

Abstract: An efficient and fast way to measure photoelectron diffraction data over the full 2 angular range with high data point density is presented, taking advantage of the massive parallel detection capabilities of modern two-dimensional electron detectors. We introduce generic routines for data binning and for the mapping of the detector signal onto emission angles. X-ray photoelectron diffraction patterns taken from Bi(1 1 1) with the new detection scheme are compared to data sets taken with a conventional hemispherical analyzer equipped with a channeltron detector. As a result, the data acquisition time can be reduced by roughly a factor of ten while obtaining comparable if not superior data quality. The sampling technique is extended to UV-excited angle-resolved photoelectron spectroscopy as illustrated by a mapping of the Fermi surface of Cu(1 1 1).

DOI: https://doi.org/10.1016/j.elspec.2014.08.007

Acquisition of photoelectron diffraction patterns with a two-dimensional wide-angle electron analyzer

Michael Greif, Luca Castiglioni, David Becker-Koch, Jürg Osterwalder, Matthias Hengsberger

Departement of Physics, University of Zürich, Winterthurerstrasse 190, CH-8057 Zürich, Switzerland

Abstract

An efficient and fast way to measure photoelectron diffraction data over the full 2π angular range with high data point density is presented, taking advantage of the massive parallel detection capabilities of modern two-dimensional electron detectors. We introduce generic routines for data binning and for the mapping of the detector signal onto emission angles. X-ray photoelectron diffraction patterns taken from Bi(111) with the new detection scheme are compared to data sets taken with a conventional hemispherical analyzer equipped with a channeltron detector. As a result, the data acquisition time can be reduced by roughly a factor of ten while obtaining comparable if not superior data quality. The sampling technique is extended to uv-excited angle-resolved photoelectron spectroscopy as illustrated by a mapping of the Fermi surface of Cu(111).

Keywords: photoelectron, diffraction, electron spectrometer, 2D detector

1. Introduction

Photoelectron diffraction is a surface structure probe that combines two unique features that make it particularly interesting for investigating bonding geometries of atoms or molecules adsorbed on surfaces and the local environment of impurity or dopant atoms inside surfaces [1, 2]. First, the diffracted electrons can be energy-selected from the x-ray photoelectron spectrum (XPS), which makes the method sensitive to the atomic type or even its specific chemical

state [3]. Second, no long-range translational order is required, therefore the molecules or the impurities do not have to be arranged on a periodic lattice. These properties set the method apart from the widely used low-energy electron diffraction (LEED) [4] method for surface structure determination. With the currently fast progressing development of pulsed light sources based on higher-harmonic generation (HHG) [5], reaching photon energies in the uv and soft x-ray region, there is also a potential to use photoelectron diffraction in a pump-probe scheme for studying structural dynamics at surfaces. Such experiments have already been successfully performed for laser-aligned molecules in the gas phase using free-electron laser pulses [6].

In photoelectron diffraction measurements, photoelectrons are emitted after absorption of either x-ray (XPD) or uv (UPD) photons, and the energy-selected intensity distribution is recorded as a function of emission direction over a large part of the 2π hemisphere above the sample. In a single-crystalline sample, where the atomic environment around equivalent emitter atoms is uniform over a macroscopic area, the interference patterns resulting from the superposition of the directly emitted photoelectron wave and those scattered by the neighboring atoms are also uniform and add up to the measured XPD/UPD pattern [1]. Such photoelectron intensity distributions provide therefore information about the atomic structure around the emitters. Figure 1 shows a typical data set in a 3D representation plotted on the surface of the scanned hemisphere.

The quality of the structural information depends on the angular resolution and sampling density, as well as the angular range covered by the measurement. A conventional hemispherical analyzer using a channeltron detector typically needs to sample several thousand points on the hemisphere, which translates into several thousand angle settings of the sample manipulator [7]. As an alternative route, parallel detection techniques were developed in the past. One approach leads to so-called display analyzers [8, 9]: in such detection schemes, the photoemission intensity distribution at a chosen electron kinetic energy is imaged onto a two-dimensional (2D) detector. This way, the diffraction pattern inside a large solid angle is measured in a parallel fashion. Despite recent im-

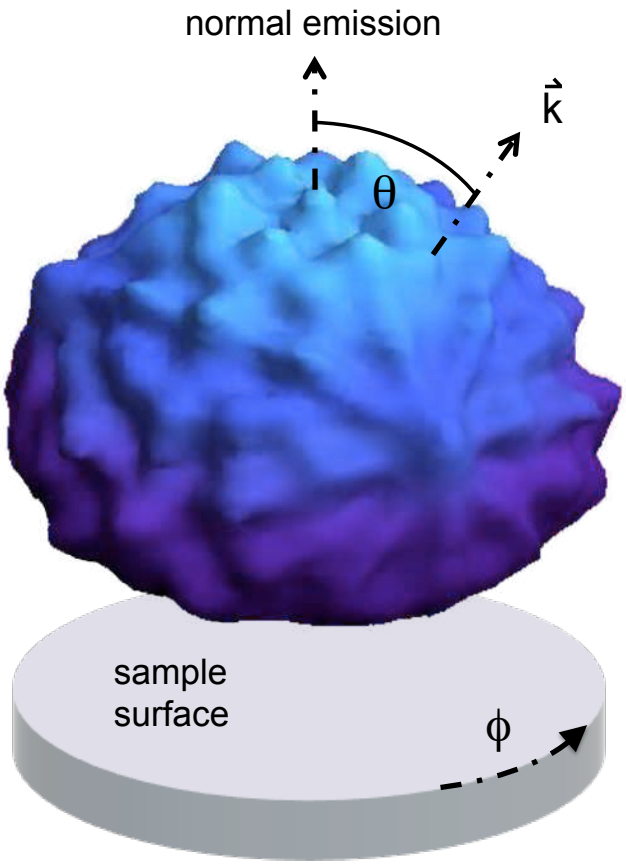

Figure 1: Photoelectron intensity distribution of Bi 4f emission, excited with photons of energy $h\nu = 1253.6$ eV, plotted on the surface of the hemisphere that is scanned with the detector. Large elevations from the spherical surface correspond to high intensities at the respective spherical angles. Normal emission and an exemplary emission direction $\vec{k}$ corresponding to the polar angle θ is indicated. ϕ shows the azimuthal rotation sense.

provements of the energy resolution (below 1% of the bandpass energy) [10] and of the acceptance angle (up to 1 sr solid angle) [11, 12] the energy scanning capabilities of such analyzers are limited. Another approach to parallel detection was the development of toroidal angle-resolving electron spectrometers with an acceptance angle of $\pm 90^\circ$ in one direction [13]. In a modern generation a range of 8% of the electron pass energy can be simultaneously recorded [14]. The mentioned analyzers are quite complex and not commercially available to the best of our knowledge.

Here we show an approach using a modern photoelectron spectrometer, with a 2D screen-CCD assembly as detector. The detector axis along the energy-dispersive direction of the electrostatic analyzer corresponds to the kinetic energy, and the intensity recorded as function of pixel position along this axis yields the energy spectrum. The simultaneously recorded energy range is 12% of the electron pass energy. The second axis perpendicular to the first one usually corresponds to a spatial emission direction of the electrons. This allows spectra to be recorded for many emission directions simultaneously. With the latest electrostatic wide-angle-acceptance lenses (WAL), the range in angle could be extended up to $\pm 30^\circ$. We present the instrumental development that permits us to use this WAL capability for the acquisition of full-hemispherical photoelectron diffraction data. In the experiments presented here, a 40° long line on the hemisphere above the sample is recorded for each angle setting rather than a single point, reducing the necessary number of settings by more than a factor of ten (see below).

Measurement times, typically of the order of a few hours for a full diffraction pattern with conventional instruments, can be reduced accordingly while maintaining similar angular resolution and statistical accuracy. Shorter measurement times are important for several reasons: on the one hand many samples are sensitive to contamination by the residual gas even under ultra-high vacuum (UHV) conditions and their surfaces degrade on the time scale of hours. On the other hand surfaces with molecular adsorbates, for instance, often suffer from radiation damage from the light sources. The damage is caused by photochemistry or

inelastic scattering of secondary electrons. Thus a faster measurement means less damage to the sample. With the advent of higher harmonics generation (HHG) a new energy regime became accessible for ultrafast laser pulses, namely the extreme ultraviolet (XUV, $h\nu \approx 20 - 100$ eV). This makes it possible to use photoelectron diffraction in a pump-probe scheme with pulsed XUV laser light as probe beam. These light sources are often only stable over a limited time span of a few hours, thereby putting another constraint on the time available for data recording. Finally, the parallel data acquisition over a line of angles makes it possible to do pump-probe experiments on specific diffraction features, identified via first taking a full diffraction pattern, without moving the sample orientation.

Here, we will show that our approach leeds to a significant reduction of measurement times while preserving or even improving the data quality.

2. Experimental Setup

The complete UHV system used in this work is shown in Fig. 2. It is built in a vertical setup with the preparation chamber on top of the analysis chamber. The base pressure in both vacuum chambers is below $p = 10^{-10}$ mbar. The preparation chamber is equipped with standard surface preparation and characterization utilities such as a low-energy electron diffraction (LEED) instrument, a quadrupole mass spectrometer, and an ion gun for sample cleaning. The chamber has several additional flanges where Knudsen cells for chemical vapor deposition can be attached. The sample manipulator is mounted on top of the two chambers along the vertical axis. It can move the sample from upper to lower chamber into the detection plane. With the goniometer mounted on the manipulator [7] the sample can also be rotated around a 2π solid angle such that the full hemisphere above the sample can be scanned with the detector. Polar angles $\theta_{Man} = 0° - 90°$ and azimuthal angles $\phi_{Man} = 0° - 360°$ can be reached. The rotations around the two axes are fully automated via two computer-controlled motors. The motors are equipped with an optical encoder and a feedback loop so that the reproducibility of the sample orientation is bet-

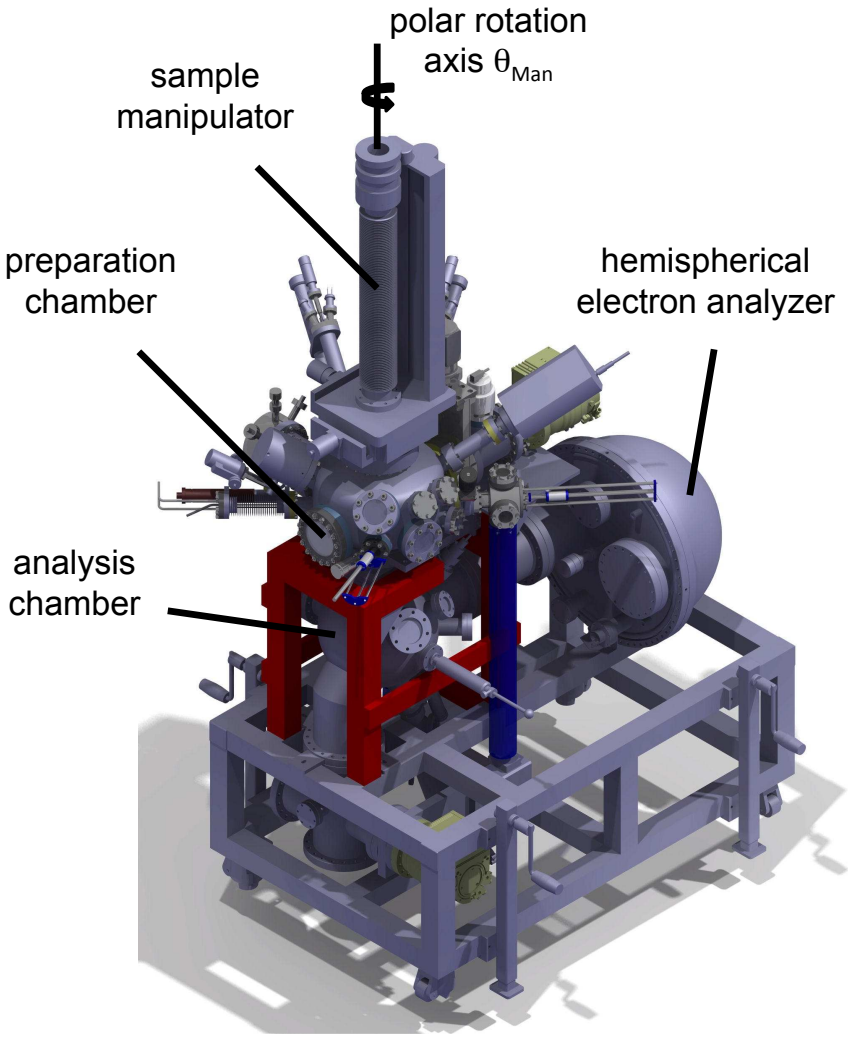

Figure 2: UHV system with surface preparation facilities and electron spectrometer. The energy-dispersive axis of the two-dimensional detector in the hemispherical analyzer is perpendicular to the polar rotation axis, the angle-dispersive axis parallel to it. Details of the detector image are shown in Fig. 3.

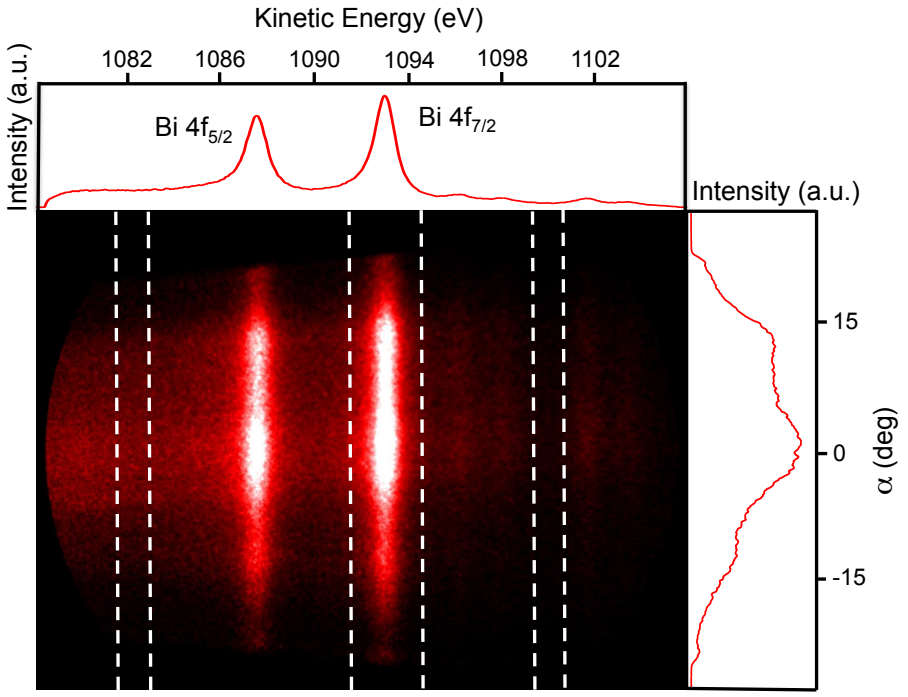

Figure 3: Snapshot of the 2D detector with the energy dispersive axis lying in the horizontal and the angular axis in vertical direction. The upper graph shows the angle-integrated energy spectrum of the two Bi 4f peaks. In the right panel the angular distribution of the Bi $4f_{7/2}$ peak integral is plotted. The integration borders are the two central dashed lines. The two lines on the low energy side and the two on the high energy side mark the areas that can be used to fit a linear or Shirley-type background [15] under the peak.

ter than 0.5°. Additionally the sample can be heated resistively and cooled by means of a liquid helium cryostat.

The analysis chamber comprises different light sources: An x-ray gun with a magnesium (Mg K_α, $h\nu = 1253.6$ eV) and a silicon anode (Si K_α, $h\nu = 1739.9$ eV), and a helium discharge lamp where both the He I_α ($h\nu = 21.2$ eV) and the He II_α line ($h\nu = 40.8$ eV) can be used. The specific angles between light incidence direction and the analyzer axis for the x-ray gun and the He lamp, respectively, are fixed in space.

A SPECS PHOIBOS 150 WAL hemispherical electron analyzer is used for electron detection. It is equipped with a wide-angle lens offering an acceptance angle of $\alpha = \pm 30°$. This angle range is imaged on the 2D detector consisting of two micro-channel plates and a screen-CCD assembly (1392 x 1024 pixels). The angular distribution of the photoelectrons is projected along the vertical direction of the detector, whereas the energy dispersive direction is along the horizontal axis, as shown in Fig. 3. The ultimate angle and energy resolution of the detector were measured to be 0.5° and 5 meV. In the data presented here the angular resolution was set to 0.5° and the energy resolution to < 200 meV.

The complete instrument is built as a compact and mobile unit that can be moved and attached to various beamlines where different light sources can be coupled into the chamber through additional viewports.

3. Reconstruction of complete diffraction patterns from single detector images

Recording full 2π photoelectron angular distributions with an energy dispersive analyzer equipped with a 2D detector is different from using a conventional detector based on channeltrons. While a channeltron detector in fixed energy mode measures the intensity at one single emission angle at a time, the WAL analyzer captures a defined energy and angular range with a single snapshot of the 2D multichannel plate (MCP) detector as shown in Fig. 3. The same figure illustrates how the photoelectron signal is obtained by integration over the energy range of the peak. The inelastic electron background can be inter-

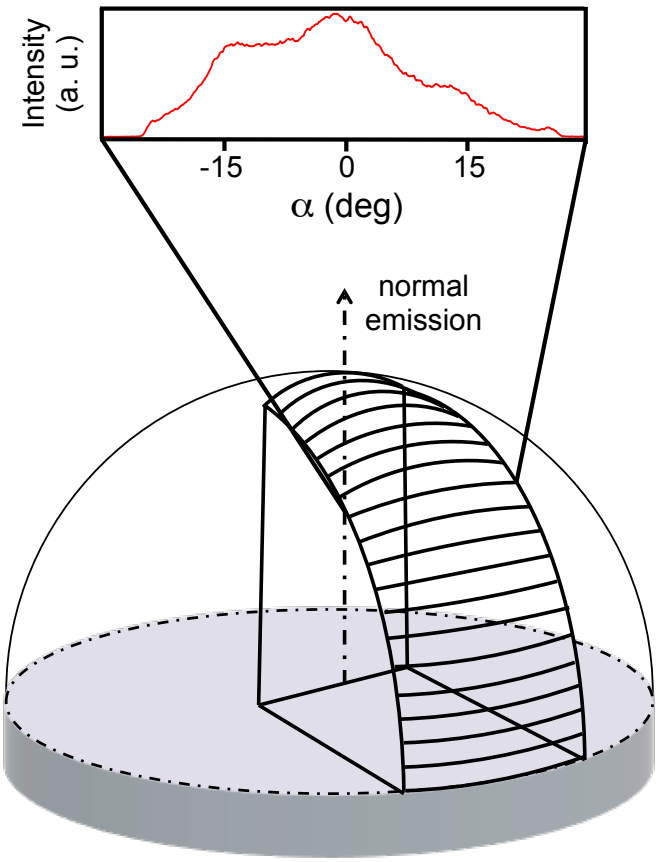

Figure 4: The Bi 4f peak on the MCP detector image is integrated and the resulting lines of intensities $I(\alpha)$, measured at different polar angles θ_{Man}, are assembled to form a broad slice out of the full 2π intensity distribution.

polated using the flat areas in the spectrum (*cf.* left and right marked areas in Fig. 3) and then be subtracted from the integral across the peak. This procedure yields the intensity distribution as a function of the detector angle $I(\alpha)$ (Fig. 4). Instead of single point measurements as in the case of a channeltron detector, the 2D detector samples data simultaneously from emission angles corresponding to a line along a great circle on the hemisphere as shown in Fig. 4. Such lines are recorded at different angular settings of the sample goniometer.

Figure 5 illustrates the angle convention used for the mapping of detector angle α and goniometer angles θ_{Man} and ϕ_{Man} onto the sample polar coordinates θ_{Sph} and ϕ_{Sph} describing the emission direction. The relation is not trivial. At $\theta_{Man} = 0°$ the line scan along the angle α coincides with a scan along the polar angle θ_{Sph} at fixed azimuthal angle ϕ_{Sph}. The other extreme is reached for $\theta_{Man} = 90°$, where the line along α becomes an azimuthal scan at constant $\theta_{Sph} = 90°$. For all other lines the relation $\theta_{Man} = \theta_{Sph}$ only holds at the detector center ($\alpha = 0°$). At detector angles $\alpha \neq 0°$ the angle set (θ_{Sph},ϕ_{Sph}) changes continously. The transformation from the sample manipulator settings θ_{Man}, ϕ_{Man} and detector angle α to the spherical emission angles θ_{Sph} and ϕ_{Sph} is given in the following two equations:

$$\theta_{Sph} = \arccos(\cos\ \alpha \cdot \cos\ \theta_{Man}\ ) \tag{1}$$

$$\phi_{Sph} = \arccos\left(\frac{\tan\ \theta_{Man}}{\tan\ \theta_{Sph}}\right) + \phi_{Man} \tag{2}$$

To sample the angular distribution over the full 2π hemisphere, we apply the following procedure: first the polar manipulator angle θ_{Man} is rotated in small steps (typically 1° or 2°) from large manipulator angles ($\theta_{Man} \leq 90°$) to normal emission ($\theta_{Man} = 0°$) in order to record a slice of intensities on the hemisphere (Fig. 4). Due to low analyzer transmission at large detector angles α, signals for $|\alpha| > 20°$ are discarded. When the first intensity slice is completed, the sample is rotated around its azimuthal angle ϕ_{Man} by 40° before taking a second slice.

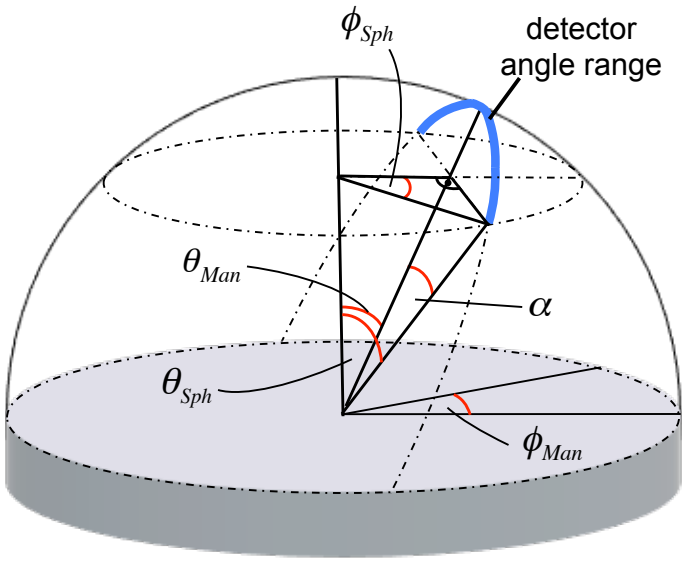

Figure 5: Overview of the characteristic angles describing the photoelectron distribution in our experimental geometry. The goniometer angles of the manipulator θ_{Man}, ϕ_{Man} and the detector angle α are converted to the spherical angles θ_{Sph} and ϕ_{Sph}. The thick blue arc indicates a single line recorded in one shot by the detector, which corresponds to a part of a great circle on the hemisphere above the sample.

Repeating this procedure nine times covers the whole range of 360° of azimuthal angles and thus the whole hemisphere. For a step size of $\theta_{man} = 2°$ this yields a total of 405 angle settings of the goniometer.

The minimum acquisition time for a complete angular distribution is given by the time that the instrument needs to move the manipulator to the correct positions and to communicate with the detector. By performing a 2 π scan with 405 angle settings with the dwell time of the data acquisition set to $t = 1$ ms, we determined the total time lag of a full scan to be 13 minutes. This is the fastest possible full 2π scan with the current setup.

For the reconstruction of the diffraction pattern it must be considered that for every energy analyzer the recorded photoelectron intensity is proportional to a device specific transmission function that will also depend on the particular mode of operation [16]. Due to the two dispersive axes (angle and energy) the transmission function of the WAL detector depends on energy and detector angle, and therefore $I(E, \alpha) \propto T(E, \alpha)$. As the diffractogram is recorded at a fixed energy, the dependence on α is of concern here. The energy dependence must be taken into account for cases in which signals at different energies are compared, like in background measurements. However, the energy dependence of T is weak in this region and energy dependent changes negligible in most cases. Since the transmission function does not depend on the orientation of the sample, a convenient way to find an approximate function for $T(\alpha)$ is to take the mean angular distribution on the detector averaged over all different sample orientations. This averaging leads to a smearing out of the diffraction pattern and reduces to the device specific transmission function $T(\alpha)$. This function is then used to normalize the measured signal $I(\alpha)$.

For graphical representation the photoelectron intensity distribution is finally projected onto a plane as shown in Fig. 6. To maintain an azimuthal conformal mapping we use the stereographic projection to convert spherical angles to polar angles on a plane where $r(\theta_{Sph})$ is the radial coordinate, ϕ_{pol} is

the angle coordinate of the plane and r_0 a scaling factor:

$$\begin{pmatrix} r(\theta_{Sph}) \\ \phi_{pol} \end{pmatrix} = \begin{pmatrix} r_0 \cdot \tan \frac{\theta_{Sph}}{2} \\ \phi_{Sph} \end{pmatrix} \tag{3}$$

In Fig. 6 the stereographic projection of a slice and the combination of slices to a full pattern is illustrated. While the left part of Fig. 6 shows only the positions of the measurement points, the right part displays the points with a color code corresponding to the intensities of a measured photoelectron diffraction pattern from a Bi(111) surface. The electrons were emitted from the Bi 4f core levels after excitation with Mg K_α photons of energy $h\nu = 1253.6$ eV. An angular step size of $\Delta\theta_{Man} = 2°$ was chosen, as this is sufficient to resolve the typical electron diffraction patterns. Along the detector angle α the minimum step size depends on the pixel density of the CCD camera. In order to reduce storage space, right at the data acquisition the pixels of the CCD raw images are binned so that $\alpha = 40°$ correspond to 64 angle channels, which results in an angular sampling density of 0.63° per angle channel. These angular scanning parameters lead to the grid of measurement points shown in Figs. 6 (a) and (b).

In Fig. 6 (b) it can be seen that for angular settings close to normal emission, i. e. close to the center of the diffraction pattern, individual slices overlap strongly. In order to have a uniform solid angle sampling density across the entire hemisphere, a data binning routine is applied where the overall point density is reduced and overlapping data points are averaged into a single data point. The optimized grid with the positions of the binned data points is presented in Fig. 6 (c). Matching the step size of the polar manipulator angle θ_{Man}, the grid points are spaced by $\Delta\theta_{Sph} = 2°$ and the step size in azimuthal angle at $\theta_{Sph} = 90°$ is $\Delta\phi_{Sph} = 2°$ and increasing for lower polar angles. The grid in Fig. 6 (c) has a constant sampling density, i. e. each point covers the same solid angle. The right panel of figure 6 (c) shows the binned data set of the Bi 4f XPD pattern from a Bi(111) surface. A three-fold symmetric diffraction pattern with distinct maxima is clearly visible.

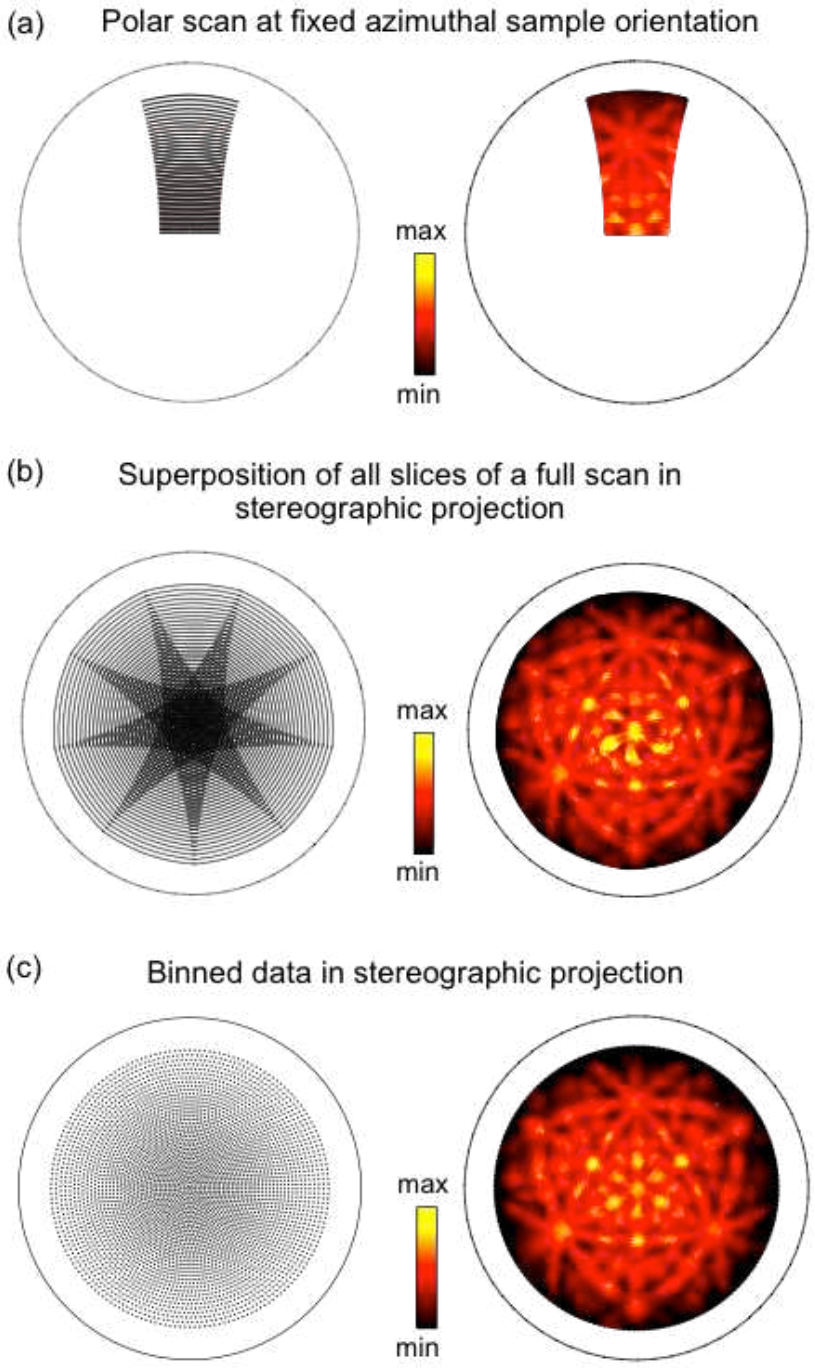

Figure 6: Reconstruction of an XPD pattern (Bi $4f_{7/2}$, $h\nu = 1253.6$ eV) in stereographic projection. The polar angle covers a range of $\Delta\theta_{Sph} = 0° - 80°$. The left panels show the grid points and the right panels the data points plotted in the corresponding color scale. (a) A single slice recorded with the WAL detector, scanning the goniometer angle θ_{Man} at fixed ϕ_{Man}. (b) Full XPD scan covering an azimuthal range of 360°, composed of 9 slices spaced at $\Delta\phi_{Man} = 40°$. (c) Same data but with intensities binned to a grid of constant solid-angle density.

4. Results

We first compare XPD data collected with the WAL analyzer, using two different data acquisition speeds, with corresponding data acquired with a conventional channeltron-based instrument [7]. In order to compensate for the weak signal at large polar angles, the XPD patterns are normalized with a fitted Gaussian function along the polar direction. As the sample has a three-fold rotational symmetry we also apply a three-fold rotational averaging. The results are shown in Figs. 7 (a) - (c), together with a corresponding simulation using single-scattering cluster theory [17]. All experimental patterns show the same diffraction features, which are furthermore well reproduced in the simulations apart from the well-known lack of feature-sharpening due to multiple-scattering effects [18].

Although the main features of the diffractogram are already visible after a total measurement time of only 15 min (a) and with a wide entrance slit (3.0 mm along the energy dispersive axis) of the analyzer, the signal is clearer after 105 min (b) where a narrow entrance slit (0.5 mm along the energy dispersive axis) of the analyzer was used. This becomes more obvious in the lower part of Fig. 7 where the anisotropies in the corresponding diffraction maps are shown for an azimuthal cut at a fixed polar angle. The anisotropy is a measure for the angular modulation depth of the signal and is defined as

$$A(\phi) = \frac{I(\phi) - I_{\min}}{I_{\max}} \tag{4}$$

where $I(\phi)$ is the azimuthal angle dependent intensity, $I_{\min}$ the minimum and $I_{\max}$ the maximum intensity along the azimuthal cut. The noise is markedly reduced when the measuring time with the WAL analyzer is increased, i.e. in going from Fig. 7 (a) to (b), and the anisotropy amplitude for a circular scan at $\theta_{Sph} = 54^\circ$ becomes larger. For comparison Fig. 7 (c) shows the same measurement with a conventional energy analyzer with a channeltron detector [7], where the overall measurement time exceeded 300 minutes. The maps in (b) and (c) look similar but the features in (b) are slightly more distinct than in (c).

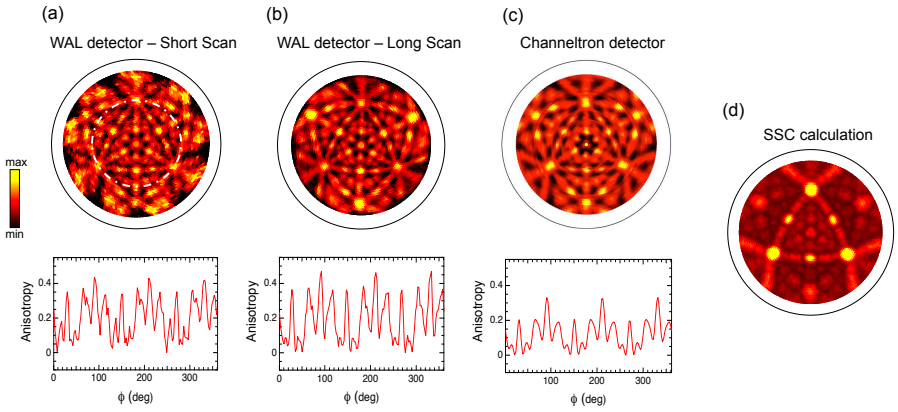

Figure 7: Comparison of different XPD measurements from Bi(111) (all data shown are taken on Bi $4f_{7/2}$ with $h\nu = 1253.6$ eV) (a) Fast XPD scan recorded with the WAL analyzer with a total measurement duration of 15 minutes. A wide entrance slit was used. (b) XPD pattern recorded with the WAL detector with narrow entrance slit and a measurement duration of 105 min. (c) XPD pattern recorded with a channeltron detector and a measurement duration of 300 min. All diffraction patterns were taken for polar angles $\theta = 0^\circ - 80^\circ$. Rotational averaging owing to the three-fold symmetry was applied and the data were normalized with a polar Gaussian function in order to reduce purely instrumental effects on the anisotropies. Below the three experimental patterns (a) through (c) the quantitative anisotropies of the corresponding data are shown *vs.* azimuthal angles ϕ_{Sph} for a circular scan at a polar angle $\theta_{Sph} = 54^\circ$ as indicated by the dashed circle in (a). (d) Single-scattering cluster (SSC) calculation of the Bi 4f XPD pattern.

This is corroborated by the anisotropy curves. They show larger anisotropies and sharper features in (b) compared to the channeltron measurement in (c). This also indicates that, for the chosen analyzer settings, the angular resolution of the WAL analyzer is superior.

While for the measurements performed with the channeltron detector the x-ray gun can be moved very close to the sample [7], this is not the case in the vacuum chamber with the WAL analyzer, which results in a lower photon flux. This can be quantified by measuring the photocurrent of the sample, which is proportional to the photon flux. The photocurrent during the WAL measurements (I_{Wal} = 21 nA) shown in Figs. 7 (a) and (b) was smaller than during those of Fig. 7 (c) (I_{Chan} = 67 nA) by a factor of 3.2. Hence with comparable photon flux, data of the quality shown in Fig.7 (b) could be measured in half an hour.

The described mapping technique works well also for lower-energy electrons emitted by uv light, in particular in angle-resolved photoelectron spectroscopy (ARPES) experiments. Fig. 8 shows a Fermi surface map of Cu(111) recorded with He I_α photons ($h\nu$ = 21.2 eV) [19]. The sp-band crossing the Fermi level and the Shockley surface state are well visible. The mirror symmetry with respect to the $\bar{M}\bar{\Gamma}\bar{M}'$ plane is lifted due to photoemission matrix element effects. The asymmetry occurs because the plane of incidence of the light does not coincide with the mirror plane of the crystal in these measurements. As a consequence, the light polarization is different for measurements on the two sides of the mirror plane.

The fact that the matrix elements are sensitive to the angle $\alpha_{\epsilon k}$ between the light polarization and the electron emission direction, and that even for unpolarized light the polarization is confined within the transversal plane perpendicular to the propagation direction, raises an issue for the data acquisition mode described in this work. In a channeltron-based instrument where one emission angle at a time is measured, $\alpha_{\epsilon k}$ is fixed for all data points. In the WAL analyzer, the detector spans a range of emission angles for a fixed goniometer position, which means that each detector angle α corresponds to a

different angle $\alpha_{\epsilon k}$. For a quantitative theoretical description this variation of $\alpha_{\epsilon k}$ along the detector has to be taken into account.

The data in Fig. 8 are projected on the parallel momentum plane ($k_{||}$-plane) of the photoelectrons for a conformal representation of $k_{||}$. The relation between spherical and planar polar angles in this case is:

$$\begin{pmatrix} r(\theta_{Sph}) \\ \phi_{pol} \end{pmatrix} = \begin{pmatrix} r_0 \cdot \sin\ \theta_{Sph} \\ \phi_{Sph} \end{pmatrix} \tag{5}$$

where $r(\theta_{Sph})$ is the radial coordinate, ϕ_{pol} is the angle coordinate on the plane and r_0 is a scaling factor.

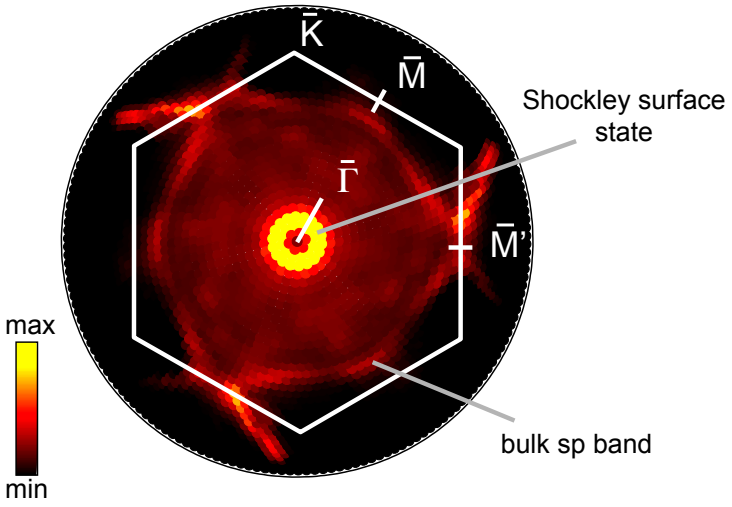

Figure 8: Fermi surface map of Cu(111) recorded with He I_α ($h\nu$ = 21.2 eV). The white hexagon indicates the borders of the first surface Brillouin zone (SBZ) with the high symmetry points $\bar{K}$, $\bar{M}$ and $\bar{M}$' indicated. The contours crossing the SBZ boundaries correspond to sections through the bulk Fermi surface while the bright circular contour near the center shows the shockley surface state [19].

5. Summary

Using a 2D detector in combination with a wide-angle lens for photoelectron diffraction measurements enables us to reduce the measurement time of diffraction maps by nearly a factor of ten in comparison with conventional instruments, while improving the data quality. The fact that for one sample orientation a wide range in angle can be covered, demands a new way to map the photoelectron intensity distribution over the 2π hemisphere above the sample. This mapping procedure is described and it is shown that the procedure works for both, high-energy (XPD) and low-energy electrons (UPD or ARPES).

The significant reduction of measurement times makes the mapping of diffraction patterns or ARPES data possible even if sample surfaces are sensitive to contamination by residual gas or to radiation damage, which both limit the sample life time. The time factor is also important when light sources, such as complex laser systems [20], have a limited stability over time.

6. Acknowledgement

We would like to thank P. Aebi, H. Daimon, T. Dienel, O. Gröning, F. Matsui, G. Monney, M. Muntwiler, J. Prinz, R. Stania and R. Widmer for fruitful discussions. Financial support of the Swiss National Science Foundation through the NCCR MUST and of the Swiss Academy of Engineering Sciences through Programme Germaine de Staël is gratefully acknowledged.

References

[1] J. Osterwalder, Surface Analysis by Auger and X-Ray Photoelectron Spectroscopy, in: D. Briggs, J. Grant (Eds.), Surface Analysis by Auger and X-Ray Photoelectron Spectroscopy, (IM Publications and Surface Spectra Limited, 2003), p. 557 ff.

[2] M. Greif, L. Castiglioni, A. P. Seitsonen, S. Roth, J. Osterwalder, M. Hengsberger, Photoelectron diffraction in the x-ray and ultraviolet regime: Sn-

phthalocyanine on Ag (111), Physical Review B 87 (2013) 085429. doi:10.1103/PhysRevB.87.085429.

[3] R. Ynzunza, F. Palomares, E. Tober, Z. Wang, J. Morais, R. Denecke, H. Daimon, Y. Chen, Z. Hussain, M. V. Hove, C. Fadley, Structure determination for saturated (1x1) oxygen on w(110) from full solid angle photoelectron diffraction with chemical-state resolution, Surface Science 442 (1999) 27 – 35. doi:10.1016/S0039-6028(99)00787-6.

[4] J. B. Pendry, Low energy electron diffraction, Academic Press London and New York, 1974.

[5] C. Spielmann, N. H. Burnett, S. Sartania, R. Koppitsch, M. Schnurer, C. Kan, M. Lenzner, P. Wobrauschek, F. Krausz, Generation of coherent X-rays in the water window using 5-femtosecond laser pulses, Science 278 (1997) 661–664. doi:10.1126/science.278.5338.661.

[6] R. Boll, D. Anielski, C. Bostedt, J. Bozek, L. Christensen, R. Coffee, S. De, P. Decleva, S. Epp, B. Erk, L. Foucar, F. Krasniqi, J. Küpper, A. Rouzée, B. Rudek, A. Rudenko, S. Schorb, H. Stapelfeldt, M. Stener, S. Stern, S. Techert, S. Trippel, M. Vrakking, J. Ullrich, D. Rolles, Femtosecond photoelectron diffraction on laser-aligned molecules: Towards time-resolved imaging of molecular structure, Physical Review A 88 (2013) 061402. doi:10.1103/PhysRevA.88.061402.

[7] T. Greber, O. Raetzo, T. J. Kreutz, P. Schwaller, W. Deichmann, E. Wetli, J. Osterwalder, A photoelectron spectrometer for k-space mapping above the Fermi level, Review of Scientific Instruments 68 (1997) 4549–4554. doi:10.1063/1.1148429.

[8] D. Eastman, J. Donelon, N. Hien, F. Himpsel, An ellipsoidal mirror display analyzer system for electron energy and angular measurements, Nuclear Instruments and Methods 172 (1980) 327 – 336. doi:10.1016/0029-554X(80)90655-2.

[9] H. Daimon, Y. Tezuka, A. Otaka, N. Kanada, S. Lee, S. Ino, H. Namba, H. Kuroda, Two-dimensional photoelectron diffraction patterns by display-type spherical mirror analyzer, Surface Science 242 (1991) 288 – 293. doi:10.1016/0039-6028(91)90281-V.

[10] H. Daimon, F. Matsui, Two-dimensional angle-resolved photoelectron spectroscopy using display analyzer—atomic orbital analysis and characterization of valence band, Progress in Surface Science 81 (2006) 367 – 386. doi:10.1016/j.progsurf.2006.05.001.

[11] L. Tóth, H. Matsuda, F. Matsui, K. Goto, H. Daimon, Details of 1π sr wide acceptance angle electrostatic lens for electron energy and two-dimensional angular distribution analysis combined with real space imaging, Nuclear Instruments and Methods in Physics Research Section A: Accelerators, Spectrometers, Detectors and Associated Equipment 661 (2012) 98 – 105. doi:10.1016/j.nima.2011.09.018.

[12] H. Matsuda, K. Goto, L. Toth, M. Morita, S. Kitagawa, F. Matsui, M. Hashimoto, C. Sakai, T. Matsushita, H. Daimon, Development of display-type ellipsoidal mesh analyzer: Computational evaluation and experimental validation, Journal of Electron Spectroscopy and Related Phenomena (2014) –doi:10.1016/j.elspec.2014.05.001.

[13] R. Leckey, J. Riley, A toroidal angle-resolving electron spectrometer for surface studies, Applications of Surface Science 22–23, Part 1 (1985) 196 – 205. doi:10.1016/0378-5963(85)90052-2.

[14] L. Broekman, A. Tadich, E. Huwald, J. Riley, R. Leckey, T. Seyller, K. Emtsev, L. Ley, First results from a second generation toroidal electron spectrometer, Journal of Electron Spectroscopy and Related Phenomena 144–147 (2005) 1001 – 1004, proceeding of the Fourteenth International Conference on Vacuum Ultraviolet Radiation Physics. doi:j.elspec.2005.01.022.

[15] D. Shirley, High-resolution X-ray photoemission spectrum of the valence bands of gold, Physical Review B 5 (1972) 4709–4714. doi:10.1103/PhysRevB.5.4709.

[16] L. Weng, G. Vereecke, M. J. Genet, P. Bertrand, W. E. E. Stone, Quantitative XPS Part I: Experimental Determination of the Relative Analyzer Transmission Function of Two Different Spectrometers - A Critical Assessment of Various Methods, Parameters Involved and Errors Introduced, Surface and Interface Analysis 20 (1993) 179–192. doi:10.1002/sia.740200302.

[17] D. Friedman, C. Fadley, Final-state effects in photoelectron diffraction, Journal of Electron Spectroscopy and Related Phenomena 51 (1990) 689 – 700. doi:10.1016/0368-2048(90)80191-C.

[18] H. Aebischer, T. Greber, J. Osterwalder, A. Kaduwela, D. Friedman, G. Herman, C. Fadley, Material dependence of multiple-scattering effects associated with photoelectron and auger electron diffraction along atomic chains, Surface Science 239 (1990) 261 – 264. doi:10.1016/0039-6028(90)90229-2.

[19] J. Osterwalder, Fermi surface mapping by photoemission, Surface Review and Letters 4 (1997) 391–408. doi:10.1142/S0218625X97000390.

[20] R. Locher, M. Lucchini, J. Herrmann, M. Sabbar, M. Weger, A. Ludwig, L. Castiglioni, M. Greif, M. Hengsberger, L. Gallmann, Versatile attosecond beamline in a two-foci configuration for simultaneous time-resolved measurements, Review of Scientific Instruments 85 (2014) 013113. doi:10.1063/1.4862656.